Journal of Alloys and Compounds 512 (2012) 361–365

Contents lists available at SciVerse ScienceDirect

Journal of Alloys and Compounds

journal homepage: www.elsevier.com/locate/jallcom

Luminescent and magnetic properties of $YVO_4:Ln^{3+}@Fe_3O_4$ ($Ln^{3+} = Eu^{3+}$ or Dy^{3+}) nanocomposites

Deming Liu, Lizhu Tong, Jianhui Shi, Hua Yang*

College of Chemistry, Jilin University, Changchun 130012, China

ARTICLE INFO

Article history:
Received 23 August 2011
Received in revised form
26 September 2011
Accepted 29 September 2011
Available online 8 October 2011

Keywords:
YVO_4:Eu
YVO_4:Dy
Fe_3O_4
Magnetic
Luminescent
Nanocomposites

ABSTRACT

A series of core–shell bifunctional magnetic–optical $YVO_4:Ln^{3+}@Fe_3O_4$ ($Ln^{3+} = Eu^{3+}$ or Dy^{3+}) nanocomposites have been successfully synthesized via two-step method. The nanocomposites have the advantage of high magnetic responsive and unique luminescence properties. The structure, luminescent and magnetic properties of the nanocomposites were investigated by XRD, TEM, PL and VSM. The maximum emission peaks of the nanocomposites are at 618 nm (doping Eu^{3+}), 574 nm (doping Dy^{3+}). The special saturation magnetization of the nanocomposites is 54 emu/g. The diameter of the nanocomposites is 400–900 nm.

1. Introduction

In recent years, bifunctional nanocomposites that exhibit significant magnetic moment and luminescence have attracted much attention because of many applications in biotechnology, medicine, and quality inspection. Bifunctional nanocomposites containing two different nanoscale functionalities might provide novel properties via the integration of fluorescent properties and magnetic nanoparticles, and therefore, offers a new potential for many applications [1–4]. Typical applications are marking and separating of cells in vitro, enhancement for magnetic resonance imaging (MRI) and subsequent optical identification, as a sensor in bioanalysis, and in the field of security code printing [5].

Bifunctional nanocomposites are composed of two main parts. One part is magnetic materials. Maghemite (Fe_2O_3) and magnetite (Fe_3O_4) have been widely used as magnetic materials in the bifunctional nanocomposites. In most cases, magnetite instead of maghemite is used because of the 25% higher magnetic saturation moment [6]. The other part is luminescent materials. Due to their good optical properties, rare-earth (RE) doped yttrium vanadate (YVO_4) as luminescent materials has been widely studied [7–10]. Investigations show that nanosized $YVO_4:Ln^{3+}$ phosphors have a significant application in a high definition flat display panel and potential applications in biology [11–13]. Consequently, some groups have been devoted to the investigation of the photoluminescence of $YVO_4:Ln^{3+}$ [14–16]. The bifunctional nanocomposites have many types, such as onion-like core–shell design and a cluster of particle's design. Core–shell type composite is typical [5]. The bifunctional magnetic–optical nanocomposites that have been reported are generally based around a core of magnetic nanoparticles [17–19]. The surface of the magnetic core is functionalised with the luminescent material. There is a disadvantage that phosphors synthesized by the sol–gel process need to be calcined, but magnetic materials as maghemite and magnetite cannot suffer high temperature. As a result, the magnetic properties of bifunctional nanoparticles are very poor.

In this paper, we present a facile hydrothermal method for the synthesis of bifunctional magnetic–optical $YVO_4:Ln^{3+}@Fe_3O_4$ ($Ln^{3+} = Eu^{3+}$ or Dy^{3+}) nanoparticles with core–shell structures. A series of lanthanide (Eu^{3+}, Dy^{3+}) ions doped yttrium vanadate phosphors were synthesized using a sol–gel method. The phosphor nanoparticles as cores were further coated with magnetite nanoparticles synthesized by a hydrothermal method. The nanocomposite particles were characterized using XRD, TEM, PL, and VSM.

2. Experimental

2.1. Materials

Ferrous chloride tetrahydrate ($FeCl_2{\cdot}4H_2O$) (99%) were purchased from Alfa Aesar Co. Y_2O_3 (99.9%), Eu_2O_3 (99.9%), and Dy_2O_3 (99.9%) were purchased from Beijing chemical plat. Sodium acetate (NaAc), ammonium metavanadate (NH_4VO_3),

* Corresponding author. Tel.: +86 431 85167712.
E-mail address: huayang86@sina.com (H. Yang).

0925-8388/$ – see front matter © 2011 Elsevier B.V. All rights reserved.
doi:10.1016/j.jallcom.2011.09.100

citric acid monohydrate, ethanol, and ammonia aqueous (25 wt%) (Shanghai Chem. Reagent Co.) are all of analytic reagents and were used as supplied.

2.2. Synthesis of rare-earth doped yttrium vanadate phosphors

YVO_4:Eu^{3+}, Dy^{3+} phosphors were synthesized using the sol–gel method. The doping concentration of the Eu^{3+} or the Dy^{3+}, respectively was 1–9 mol% or 0.5–3 mol% in the yttrium vanadate. In a typical procedure, stoichiometric amounts of Y_2O_3, Eu_2O_3 or Dy_2O_3 and citric acid were dissolved in dilute nitric acid with heating followed by the addition of NH_4VO_3 in distilled water. The solution was continuously stirred at 80 °C for several hours until it turned to sticky blue sol, and the sol was dried at 120 °C for 24 h to obtain the blue gel. The gel was pre-calcination at 500 °C for 2 h, and then calcined at 900 °C or 1000 °C for 4 h to obtain the phosphor samples. The sintered powder samples were then used for the further preparation steps.

2.3. Synthesis of Fe_3O_4-encapsulated phosphor particles

The Fe_3O_4-encapsulated phosphor particles were synthesized by a hydrothermal method. 0.1 g phosphor particles and 0.25 g CTAB were introduced into 40 ml water with stirring. Then 1 g $FeCl_2$ was dissolved in the solution. That solution was stirring for 10 min, then 5 g NaAC was added into the solution. After stirring for 30 min, transferred the mixture into an autoclave and treated by heating to 180 °C for 6 h. The precipitate formed was separated with magnet from the solution, then washed with distilled water and ethanol for several times. The final product was dried at 50 °C in the air for 8 h.

The Fe_3O_4 sample used in the VSM test is synthesized by the same method.

2.4. Characterization

The purities of all the samples were checked by X-ray diffraction measurements at room temperature using CuKα radiation (Kα = 1.54059 Å). A spectrophotometer (Shimadzu RF-5301 PC spectrofluorometer equipped with a 150 W xenon lamp as the excitation source.) was used for the photoluminescent (PL) measurement at room temperature. Magnetic measurements were determined using a vibrating sample magnetometer (VSM) (Digital Measurement System JDM-13) with a maximum magnetic field of 10,000 Oe. Transmission electron microscopy (TEM) images were observed under a JEOL-2010 electron microscope operating at 200 kV.

3. Results and discussion

We have successfully synthesized bifunctional magnetic–optical YVO_4:Ln^{3+}@Fe_3O_4 (Ln^{3+} = Eu^{3+} or Dy^{3+}) nanocomposites. The formation process is illustrated in the Scheme 1. Firstly, the YVO_4:Eu^{3+}, Dy^{3+} phosphors were synthesized by a sol–gel method. Secondly, Fe_3O_4 nanoparticles were prepared by a hydrothermal method, and coated on the surface of the YVO_4:Ln^{3+} phosphor nanoparticles. YVO_4:Ln^{3+}@Fe_3O_4 (Ln^{3+} = Eu^{3+} or Dy^{3+}) phosphors are as a core and Fe_3O_4 nanoparticles are as a shell.

Fig. 1 shows the XRD patterns of YVO_4:Eu^{3+} (a); YVO_4:Eu^{3+}@Fe_3O_4 (b) (X = 0.01, 0.03, 0.05, 0.07, 0.09); YVO_4:Dy^{3+} (c); and YVO_4:Dy^{3+}@Fe_3O_4 (d) (X = 0.005, 0.01, 0.02, 0.03) nanocomposites were annealed at 1000 °C (a and b) and 90 °C (c and

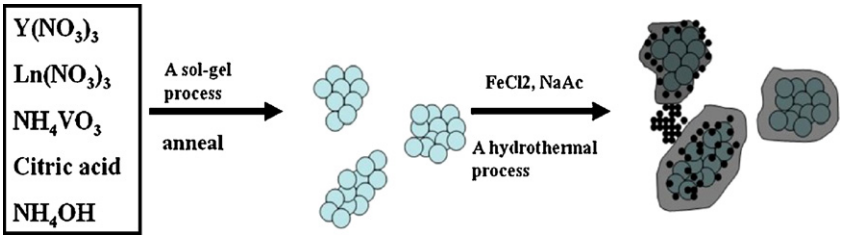

Scheme 1. Illustration for formation process of YVO_4:Ln^{3+}@Fe_3O_4 nanocomposites.

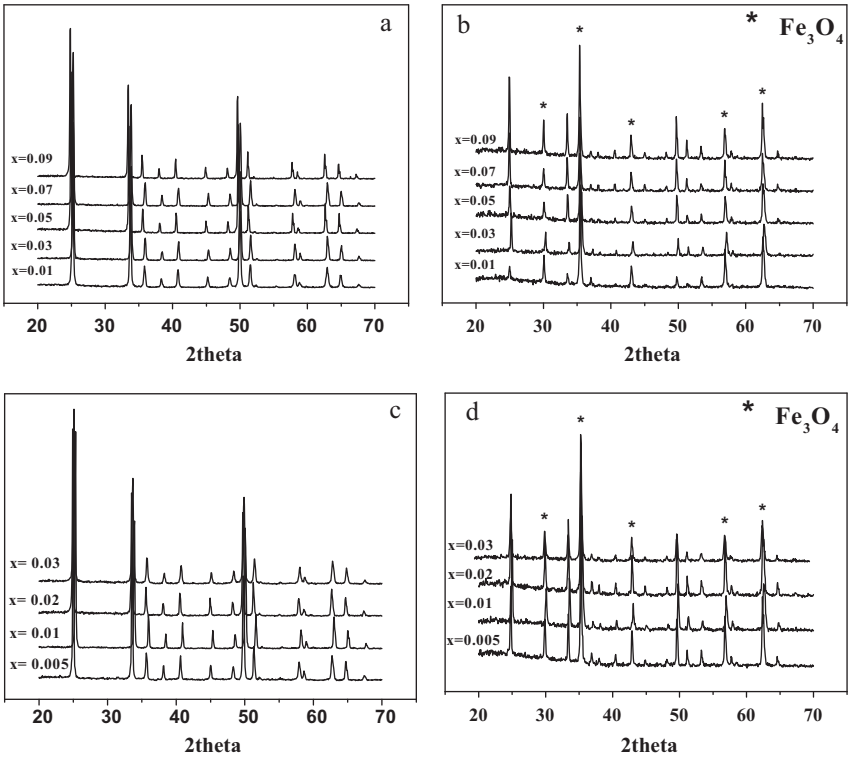

Fig. 1. XRD patterns of YVO_4:Eu^{3+} (a); YVO_4:Eu^{3+}@Fe_3O_4 (b); YVO_4:Dy^{3+} (c) and YVO_4:Dy^{3+}@Fe_3O_4 (d).

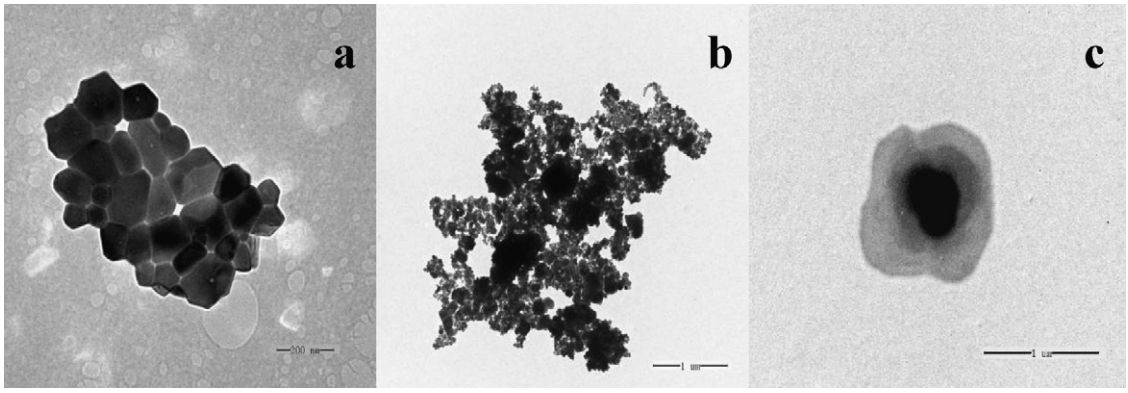

Fig. 2. TEM micrographs of YVO_4:Eu^{3+} (a) and YVO_4:Eu^{3+}@Fe_3O_4 (b and c).

d). The XRD diffraction peaks of the YVO_4:Eu^{3+} (a) and YVO_4:Dy^{3+} (c) nanoparticles can be indexed according to the standard data of YVO_4 (JCPDS 17-0341), suggesting the successful crystallization of YVO_4:Ln^{3+} with different Ln^{3+} doping concentration. The main XRD diffraction peaks at $2\theta = 25^\circ$, 33.5°and 50° are, respectively due to the (2 0 0), (1 1 2), (3 1 2) reflection of YVO_4. Fig. 1(b and d) shows the XRD patterns of Fe_3O_4-encapsulated phosphors. The XRD diffraction peaks at $2\theta = 30^\circ$, 35.4°, 43°, 57° and 62.5° of Fe_3O_4 can be indexed to face-centered structure, which is close to the report data (JCPDS 85-1436). The Fe_3O_4 had been successful synthesized in the sample of YVO_4:Ln^{3+} phosphors.

Fig. 2 shows the photoluminescence spectrum of YVO_4:Eu^{3+} (a and b) and YVO_4:Eu^{3+}@Fe_3O_4(c and d). For the excitation spectrum of YVO_4:Eu^{3+}, there is a broad band at 323 nm in Fig. 2(a). The band can be attributed to a charge transfer through the V–O bond overlay the Eu–O charge transfer band. From molecular orbital theory, the band is the transitions from ground state $^1A_2(^1T_1)$ to excited states $^1A_1(^1E)$ and $_1E(^1T_2)$ of VO_4^{3-} complexes. Three main bands at 397 nm, 467 nm and 538 nm are corresponding to the electron transitions from the $^7F_0$–$^5L_6$, $^7F_0$–$^5L_2$ and $^7F_0$–$^5L_1$, respectively. This phenomenon demonstrates the presence of an energy transfer from VO_4^{3-} groups to Eu^{3+} [20,21]. However,

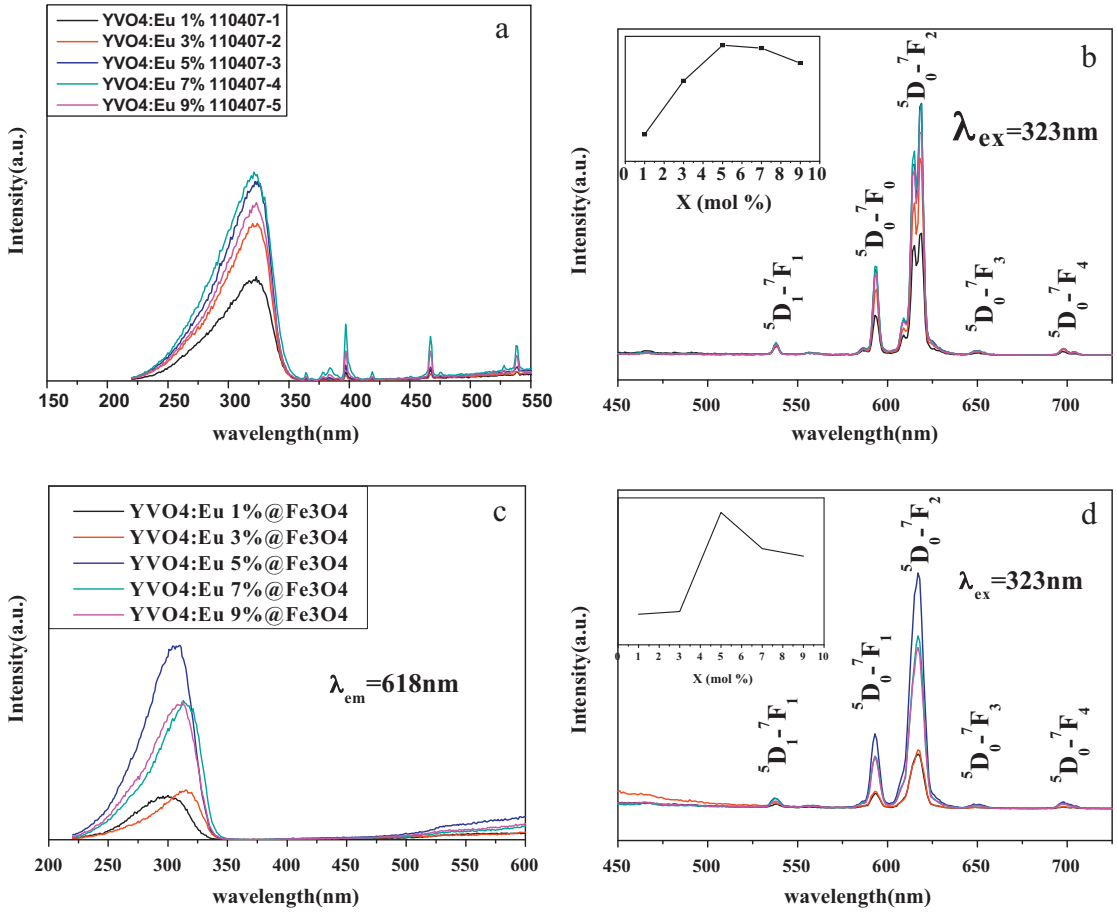

Fig. 3. Excitation spectra of YVO_4:Eu^{3+} (a), YVO_4:Eu^{3+}@Fe_3O_4 (c); emission spectra of YVO_4:Eu^{3+} (b); YVO_4:Eu^{3+}@Fe_3O_4 (d); the insets of (b) and (d) are plots of emission intensity at 618 nm variation with various Eu^{3+} doping concentration.

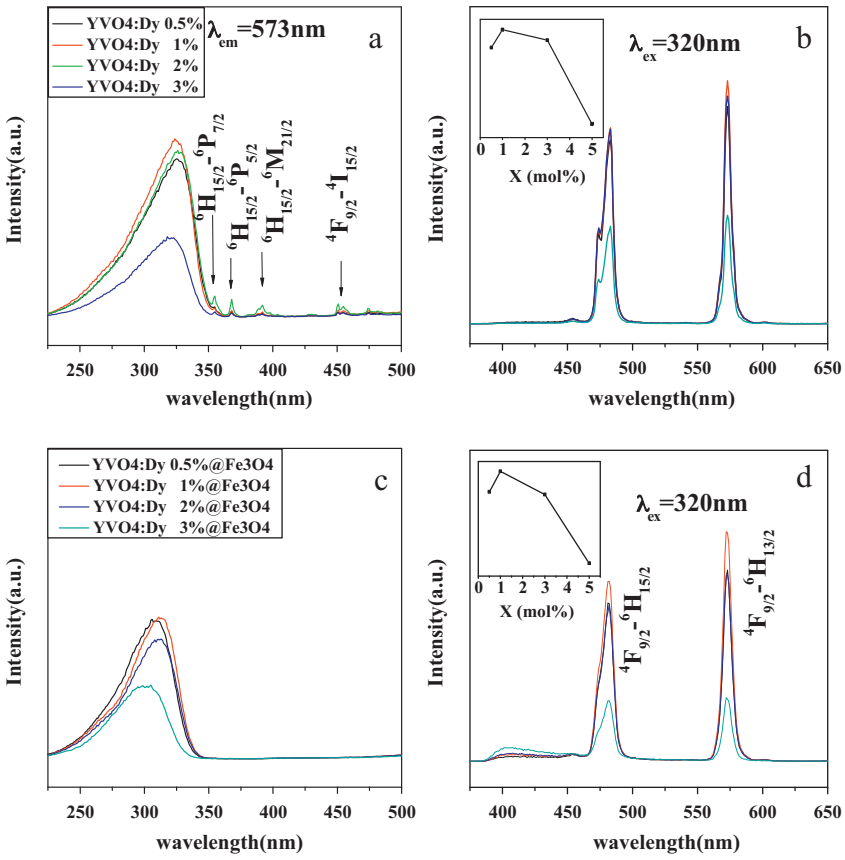

Fig. 4. Excitation spectra of YVO_4:Dy^{3+} (a), YVO_4:Dy^{3+}@Fe_3O_4 (c); emission spectra of YVO_4:Dy^{3+} (b); YVO_4:Dy^{3+}@Fe_3O_4 (d); the insets of (b) and (d) are plots of emission intensity at 573 nm variation with various Dy^{3+} doping concentration.

when the YVO_4:Eu^{3+} phosphors were coated with Fe_3O_4 nanoparticles in Fig. 2(c), there are not the three peaks. That is probably due to the energy transfer from VO_4^{3-} groups to Eu^{3+} absorbed by Fe_3O_4 nanoparticles. The emission spectra of YVO_4:Eu^{3+} are shown in Fig. 2(b). The main emission peaks at 618 nm and 593 nm are resulted from the $^5D_0$–$^7F_2$ transition and $^5D_0$–$^7F_1$ transition of Eu^{3+} ions in the YVO_4. It is well known that when the Eu^{3+} ion in the YVO_4 is located at a crystallographic site without inversion symmetry, the transition $^5D_0$–$^7F_2$ red emission will dominate in the emission spectrum. The inset of Fig. 2(b) is plots of emission intensity at 618 nm variation with various Eu^{3+} doping concentration. The optimum doping concentration of Eu^{3+} ions is 5 mol% according to the inset. This is consistent with previous reports [22]. After coated Fe_3O_4, the optimum doping concentration is still 5 mol% in the inset of Fig. 2(d).

The photoluminescence spectra of YVO_4:Dy^{3+} (a and b) and YVO_4:Dy^{3+}@Fe_3O_4 (c and d) are shown in Fig. 3. The excitation spectrum in Fig. 3(a) consists of abroad, intense band ranging from 225 to 350 nm with a maximum 320 nm and weak lines in the longer wavelength region. It is similar to the excitation spectra of YVO_4:Eu^{3+}. The band can be attributed to a charge transfer through the V–O bond overlay the Dy–O charge transfer band. Four main peaks at 351 nm, 367 nm, 386 nm, 454 nm correspond to the electron transitions from $^6H_{15/2}$ state to $^6P_{7/2}$, $^6P_{5/2}$, $^6M_{21/2}$, $^4I_{15/2}$. After the YVO_4:Dy^{3+} phosphor-coated Fe_3O_4, the peaks also disappear. That may be due to the energy transfer from VO_4^{3-} groups to Dy^{3+} absorbed by ferrite. The emission spectra of YVO_4:Dy^{3+} are shown in Fig. 3(b). The main emission peaks at 484 nm, 574 nm are resulted from the $^4F_{9/2}$–$^6H_{15/2}$ transition and $^4F_{9/2}$–$^6H_{13/2}$ transition of Dy^{3+} ions. The insets of Fig. 3(b and d) are plots of emission peak intensity at 574 nm variation with various Dy^{3+} doping concentration. The optimum doping concentration of Dy^{3+} ions is 1 mol%.

TEM images of YVO_4:Eu^{3+}@Fe_3O_4 are shown in Fig. 4. From Fig. 4(a), we can observe that the particle sizes of the as-prepared YVO_4:Eu^{3+} are from 40 to 180 nm. After coated Fe_3O_4 on the surface of YVO_4:Eu^{3+}, the particle sizes of YVO_4:Eu^{3+}@Fe_3O_4 becomes about 400–900 nm in Fig. 4(b and c). From Fig. 4(c), we can see the core–shell structure of YVO_4:Eu^{3+}@Fe_3O_4, which core is YVO_4:Eu^{3+} phosphor and shell is Fe_3O_4.

Fig. 5 is magnetization loops of Fe_3O_4 and YVO_4:Eu^{3+}@Fe_3O_4 nanocomposites at room temperature. The special saturation magnetization Ms of Fe_3O_4 nanoparticle is 80 emu/g in Fig. 5(a), which is lower than 92 emu/g of bulk Fe_3O_4. The Ms of YVO_4:Eu^{3+}@Fe_3O_4 nanocomposites is about 54 emu/g in Fig. 5(b). It is lower than the Ms of pure Fe_3O_4 nanoparticle. The large drop in saturation magnetization per gram in the bifunctional nanocomposites is due to the presence of the nonmagnetic phosphor phase.

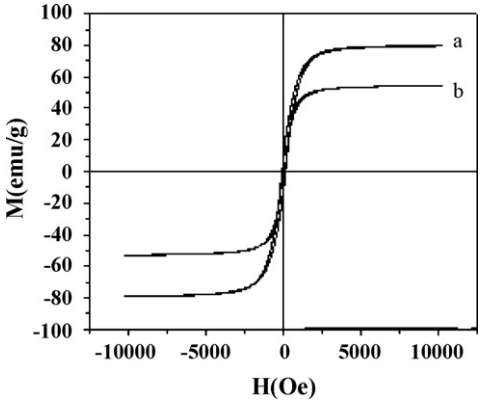

Fig. 5. Magnetization loops of Fe_3O_4 (a) and YVO_4:Eu^{3+}@Fe_3O_4 (b).

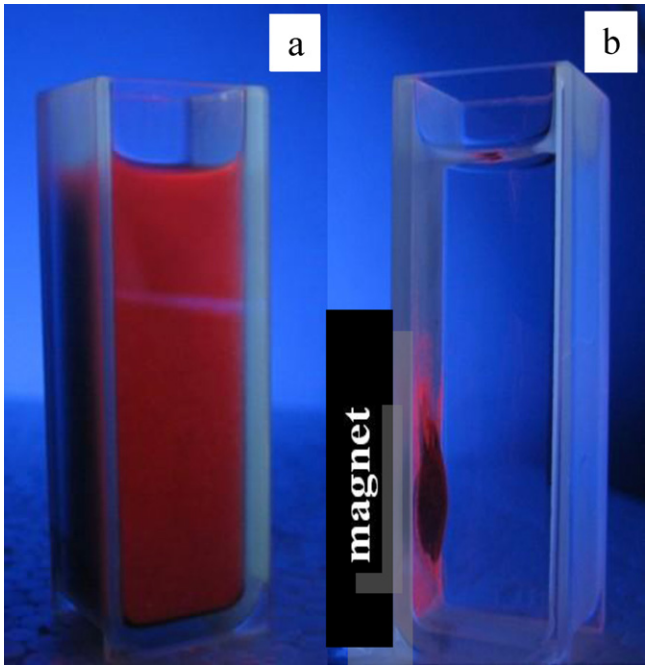

Fig. 6. Photographs of YVO_4:Eu^{3+}@Fe_3O_4 dispersed in the ethanol under UV excitation at 323 nm without (a) and with (b) external magnetic field.

Fig. 6 shows photographs of an YVO_4:Eu^{3+}@Fe_3O_4 dispersed in the ethanol under UV excitation at 323 nm without and with an external magnetic field. In Fig. 6(a), we can see that the YVO_4:Eu^{3+}@Fe_3O_4 nanocomposites well disperse in the ethanol, and emit obvious red luminescence. When we put the Fe_3O_4 magnet on the sample pool, the nanocomposites accumulate near the magnet and still emit red light. There is no light in the ethanol. These photographs can prove that we have successfully synthesized bifunctional magnetic–optical nanoparticles.

4. Conclusions

In this paper, we were successfully synthesized a series of bifunctional magnetic–optical YVO_4:Eu^{3+}@Fe_3O_4 and YVO_4:Dy^{3+}@Fe_3O_4 nanoparticles with core–shell structure via two-step method. The optimum concentration of Eu^{3+} and Dy^{3+} ions in YVO_4 host is 5 mol% and 1 mol%, respectively. The maximum emission peaks of YVO_4:Eu^{3+}@Fe_3O_4 and YVO_4:Dy^{3+}@Fe_3O_4 nanocomposites are at 618 and 574 nm, respectively. The particle sizes of the YVO_4:Ln^{3+}@Fe_3O_4 (Ln^{3+} = Eu^{3+}, Dy^{3+}) nanoparticles are 400–900 nm. The special saturation magnetization of the nanocomposite is 54 emu/g. With the advantage of high magnetic responsive, unique luminescence properties, these YVO_4:Eu^{3+}@Fe_3O_4 and YVO_4:Dy^{3+}@Fe_3O_4 nanocomposites could be used in marking and separating of cells in vitro, enhancement for magnetic resonance imaging (MRI) and subsequent optical identification.

Acknowledgement

This work is supported by National Natural Science Foundation of China.

References

[1] H. Zeng, J. Li, J.P. Liu, Z.L. Wang, S.H. Sun, Nature 420 (2002) 395–398.
[2] X. He, Y. Liu, H. Li, H. Huang, J. Liu, Z. Kang, S.-T. Lee, J. Colloid Interface Sci. 356 (2011) 107–110.
[3] H. Wang, Y. Li, L. Sun, Y. Li, W. Wang, S. Wang, S. Xu, Q. Yang, J. Colloid Interface Sci. 350 (2010) 396–401.
[4] M. De, P.S. Ghosh, V.M. Rotello, Adv. Mater. 20 (2008) 4225.
[5] D. Vollath, Adv. Mater. 22 (2010) 4410.
[6] X. Yu, Y. Shan, G. Li, K. Chen, J. Mater. Chem. 21 (2011) 8104.
[7] M. Wen, W. Zhao, T. Zhang, Y. Zhu, Y. Wang, Q. Wu, J. Colloid Interface Sci. 322 (2008) 143–151.
[8] V. Buissette, D. Giaume, T. Gacoin, J.-P. Boilot, J. Mater. Chem. 16 (2006) 529.
[9] L. Li, M. Zhao, W. Tong, X. Guan, G. Li, L. Yang, Nanotechnology 21 (2010) 195601.
[10] W. Wang, Z. Cheng, P. Yang, Z. Hou, C. Li, G. Li, Y. Dai, J. Lin, Adv. Funct. Mater. 21 (2011) 456.
[11] L. Sun, Y. Zang, M. Sun, H. Wang, X. Zhu, S. Xu, Q. Yang, Y. Li, Y. Shan, J. Colloid Interface Sci. 350 (2010) 90–98.
[12] P. Govindaiah, Y.J. Jung, J.M. Lee, T.-J. Park, D.Y. Ryu, J.H. Kim, I.W. Cheong, J. Colloid Interface Sci. 343 (2010) 484–490.
[13] F. Wang, X. Xue, X. Liu, Angew. Chem. Int. Ed. 47 (2008) 906.
[14] M. Zhang, H. Fan, B. Xi, X. Wang, C. Dong, Y. Qian, J. Phys. Chem. C 111 (2007) 6652.
[15] G. Jia, Y. Song, M. Yang, Y. Huang, L. Zhang, H. You, Opt. Mater. 31 (2009) 1032–1037.
[16] F. He, P. Yang, N. Niu, W. Wang, S. Gai, D. Wang, J. Lin, J. Colloid Interface Sci. 343 (2010) 71–78.
[17] J. Gao, B. Zhang, Y. Gao, Y. Pan, X. Zhang, B.J. Xu, Am. Chem. Soc. 129 (2007) 11928.
[18] L. Zhang, B. Liu, S. Dong, J. Phys. Chem. 111 (2007) 10448.
[19] Z. Sun, D. Liu, L. Tong, et al., Solid State Sci. 13 (2011) 361–365.
[20] L. Li, M. Zhao, W. Tong, et al., Nanotechnology 12 (2010) 195601.
[21] A. Bao, H. Lai, Y. Yang, et al., J. Nanopart. Res. 12 (2010) 635–643.
[22] A. Huignard, et al., Chem. Mater. 12 (2000) 1090–1094.